Preparation of a TiO_2–MoS_2 nanoparticle-based composite by solvothermal method with enhanced photoactivity for the degradation of organic molecules in water under UV light

I. Tacchini[1], *E. Terrado*[1,2], *A. Ansón*[1], *M.T. Martínez*[1]

[1]*Instituto de Carboquímica, CSIC, Miguel Luesma Castán 4, 50018 Zaragoza, Spain*
[2]*Facultad de Ciencias de la Salud, Universidad de San Jorge, Villanueva de Gallego, 50830 Zaragoza, Spain*
E-mail: itac@icb.csic.es

Published in Micro & Nano Letters; Received on 31st August 2011; Revised on 23rd October 2011

The MoS_2 nanocrystals coupled with anatase nanoparticles were prepared by the solvothermal method at relatively low temperatures. It was determined that the materials consisted of 15–20 nm diameter anatase nanoparticles with highly dispersed MoS_2 nanocrystals of approximately 3–7 nm in size. Visible light absorption in the MoS_2–TiO_2 samples increased with the MoS_2 content. However, their lambda edges (λ_{edge}) remained almost identical at approximately 390 nm, meaning that MoS_2 did not cause a red shift in the anatase bandgap energy. The hybrid MoS_2-anatase materials had higher surface area (70–124 $m^2\,g^{-1}$) than commercial TiO_2 (P25) (50 $m^2\,g^{-1}$). The MoS_2-anatase hybrid nanocrystals showed enhanced activity in the oxidation of methylene blue in water under UV light irradiation. A photomechanism able to elucidate the observed dye decolourisation was suggested.

1. Introduction: Titanium dioxide nanoparticles (TiO_2–NPs) are interesting photoactive nanostructure materials with a promising future owing to their potential application for photovoltaic cells [1], hydrogen production by water splitting [2], environmental photocatalysis [3] and self-cleaning surfaces [4].

It has been demonstrated [5] that several structural parameters such as morphology, particle size, crystallinity and surface features strongly influence the properties of TiO_2–NPs. Such parameters are determined by the synthesis method and the post-treatments (e.g. thermal post-treatment to improve crystallinity). The most popular synthesis techniques are sol–gel processes [6], hydrothermal and solvothermal methods [7].

Absorption of a photon with sufficient energy by a TiO_2 crystal leads to a charge separation owing to an electron promotion to the conduction band and a resulting hole in the valence band [8]. This hole can be used to oxidise organic compounds onto the surface of the TiO_2 crystal. Nevertheless, the photocatalytic efficiency of TiO_2 towards organic compounds degradation can substantially decrease as a result of the high recombination ratio of photo-induced electron-hole pairs generated under UV radiation.

The modification of TiO_2–NPs with inorganic substances, such as noble metals [9], transition metals [10], non-metals [11] and semiconductors [12], has been considered for maximising its photocatalytic efficiency. These dopers work by favouring the electron-hole separation and promoting the interfacial electron transfer [13], decreasing TiO_2 bandgap (which benefits the electron transfer from valence band to conduction band [14]) or increasing the activity of TiO_2 by extending the wavelength range response of TiO_2 to the visible region [15]. Unfortunately, dopers can also operate as electron-hole recombination centres that are detrimental to photocatalytic activity [16].

On the other hand, coupling on the crystal surface with metals [16], non-metals [17] or semiconductors [12] has positive effects, with a heterostructure being generated on the interface between TiO_2 and semiconductor NPs that is beneficial to enhancing the separation efficiency of the photogenerated electron-hole pair.

In this respect, combining semiconductors with a small bandgap, such as CdS [12] or Bi_2S_3 [18], with TiO_2 helps the photogenerated electron in the small bandgap semiconductor transfer to the TiO_2 particles, while the holes remain in the particles of the other coupling materials. Owing to the values of energy in the conduction and valence band of MoS_2 [19] compared to anatase, MoS_2 works in a way that is different from CdS or Bi_2S_3. MoS_2 could accept the photogenerated electron from TiO_2 while keeping the hole separated from the electron. Additionally, MoS_2 shows several particular advantages over CdS and Bi_2S_3 that should be considered. First of all, the electronic states of the conduction and valence bands in bulk MoS_2 are derived from the electronic structure of Mo (4d orbital), so photoexcitation of electrons should not weaken Mo–S bonds, which are responsible for the photostability of MoS_2 during photo-oxidation of water [20]. Moreover, if the size of MoS_2 is reduced to the nanoscale, edge-site Mo atoms are not protected by the inert basal planes of MoS_2. As a result, the bandgap of the MoS_2 nanocrystals becomes small enough to allow a wider range of the solar spectrum to be collected [21].

In contrast to CdS, MoS_2 nanoparticles are considerably stable in water. The lattice dissolution process via the oxidation of sulphur to a sulphate ion is slower in a covalent material such as MoS_2, compared to an ionic semiconductor such as CdS [22]. Thus, it would be possible for MoS_2 nanoparticles to be employed in waste water treatments.

This Letter describes a simple method for coupling MoS_2 nanocrystals with TiO_2–NPs we have developed to obtain a hybrid nanostructured material with enhanced activity for the degradation of organic molecules in water under UV light.

2. Materials and methods: TiO_2–NPs were prepared by a combination of sol–gel and solvothermal methods. In a typical experiment, 5 ml of titanium isopropoxide (Aldrich) were diluted in 45 ml of 2-propanol. The solution was added drop-wise into a mixture consisting of 26 ml of 2-propanol with 26 ml of water. In contact with aqueous medium, titanium isopropoxide decomposes to form non-crystalline TiO_2–NPs. The resulting powders were aged overnight in the reaction mixture, then filtered and washed with distilled water, and dried at 105°C for 24 h.

For the synthesis of hybrid materials, the previously prepared TiO_2–NPs were mixed with different quantities (0, 2, 5, 7.5 and 10 weight%) of MoS_2 (Aldrich) in 20 ml of a 1/1 (volumetric ratio) water/2-propanol solution and strongly stirred for 2 h. The mixtures were then thermally treated in a 25 ml autoclave (200°C, 35 bar) for 24 h in order to convert amorphous TiO_2–NPs into crystal anatase-NPs. The obtained materials were filtered, rinsed with distilled water and dried at 105°C for 24 h. MoS_2 content in the hybrid materials were confirmed by scanning electron microscopy–energy-dispersive X-ray spectroscopy (SEM-EDX) measures (0, 2.3, 5.6, 7.1 and 12 weight%).

doi: 10.1049/mnl.2011.0460

The nanostructures were characterised by transmission electron microscopy (TEM, JEOL-200FXII), SEM-EDX (Hitachi S3400N-Röntech) X-ray diffraction (XRD) (Bruker AXS D8 advance diffractometer), nitrogen adsorption (Micromeritics ASAP 2020) and UV–vis absorption (UV–VIS Spectrometer Shimadzu UV-3600 equipped with a labsphere diffuse reflectance accessory) and elemental analysis (Carlo Erba 1108).

3. Results and discussions

3.1. Characterisation: XRD spectra (Fig. 1) revealed a pattern of broad peaks, characteristic of small particle sizes. Two small and broad peaks were found at 13.5° and 33–35° in the XRD spectra for all the samples containing MoS_2. According to the literature, such peaks are related to the (002) and (100) crystallographic planes [23] in the hexagonal structure of MoS_2. Furthermore, the diffractogram of all the samples showed the characteristic peaks of anatase (the most photoactive crystalline form of TiO_2 [24]), which were found at 25.5°, 37.3°, 38°, 39.8°, 48.25°, 54.2, 55.4°, 62.9°, corresponding to its (101), (103), (004), (112), (200), (105), (211), (204) crystallographic planes [25].

Crystal size was calculated by using the Scherrer formula. The average crystal size (Table 1) obtained for anatase from XRD data was around 20 nm for anatase-NPs and 5 nm for MoS_2–NPs. Brunauer–Emmett–Teller (BET) surface area results for MoS_2–TiO_2–NPs are listed in Table 1. The highest value is related to samples with the highest MoS_2 concentration.

It can be concluded from the TEM images analysis of the MoS_2–TiO_2–NPs samples that the anatase-NPs were agglomerated and covered with MoS_2 nanocrystals. An image from a 7.1% MoS_2 sample is shown in Fig. 2.

Diffuse reflectance UV–vis absorption spectra for the MoS_2–TiO_2–NPs are shown in Fig. 3. All the samples exhibited absorption bands in the visible region owing to MoS_2 and in the UV region owing to anatase. The absorption onsets were determined by linear extrapolation from the inflection point of the curve to the baseline. The edges of the absorption of the MoS_2–TiO_2–NPs samples were measured at approximately 390 nm, corresponding to bandgap energy of 3.2 eV [26]. There was no red shift when compared with anatase.

3.2. Photodecolouration activity: The photocatalytic activity of TiO_2 systems is usually evaluated by measuring the time dependence of the concentration loss of a degraded compound, commonly, dyes such as methylene blue (MB) which predicts an exponential decay of concentration as a function of time. The enhancement achieved in the MoS_2–TiO_2 composite may be evaluated by comparison with the activity relative to a standard (which is usually P25).

Nevertheless, the comparison among different series of experiments could be a complex task due to the variety of different equipments (lamps, reactors, etc.) and testing methods used in different laboratories. Although the relative activity can be well quantified for a given set of experiments, it is inaccurate using it as an independent standard for the comparison with results obtained from other studies because the way in which the kinetic parameters are obtained is inherently linked to experimental details [27].

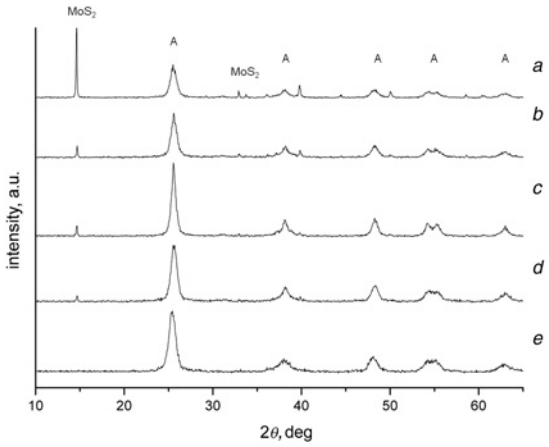

Figure 1 *XRD spectra of the TiO_2–NPs samples*
a Doped with 12% MoS_2
b Doped with 7.1%
c Doped with 5.6%
d Doped with 2.3%
e TiO_2–NPs

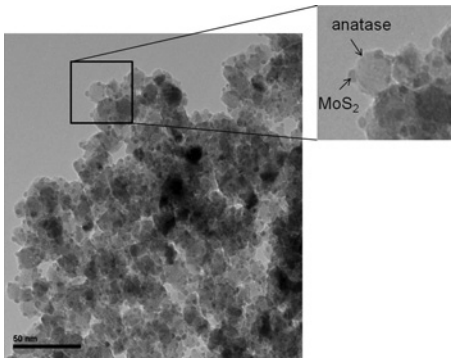

Figure 2 *TEM micrograph corresponding to the TiO_2–NPs doped with 7.1% MoS_2*

Table 1 Crystal sizes (calculated from XRD measurements using the Scherrer formula), specific surface areas calculated by the BET method and kinetic parameters (apparent first-order rate constant with R^2) for the commercial TiO_2 (P25) and the TiO_2–MoS_2–NPs with different contents of MoS_2, synergy factor R based on P25 and TiO_2 NP as growth and % of degradation and mineralisation

Sample	Cristal size, nm		Specific surface, m^2/g	Photodecomposition				
	Anatase	MoS[a]		k_{app}, min^{-1}	R^2	$R = \frac{k_{app}(TiO_2–MoS_2)}{k_{app}(P25)}$	Degradation, %	Mineralisation, %
P25	32	52	50	0.016	0.989	1.000	15	7
TiO_2 NP[b]	21	0	70	0.017	0.987	1.063	22	13
2.3% MoS_2	20	7	100	0.018	0.987	1.125	31	23
5.6% MoS_2	15	7	116	0.021	0.987	1.313	41	31
7.1% MoS_2	15	5	118	0.034	0.976	2.125	65	43
12% MoS_2	15	3	124	0.024	0.984	1.500	41	35

[a]In case of P25 MoS_2 crystal size means rutile crystal size
[b]Sample of TiO_2 nanoparticles as growth without MoS_2

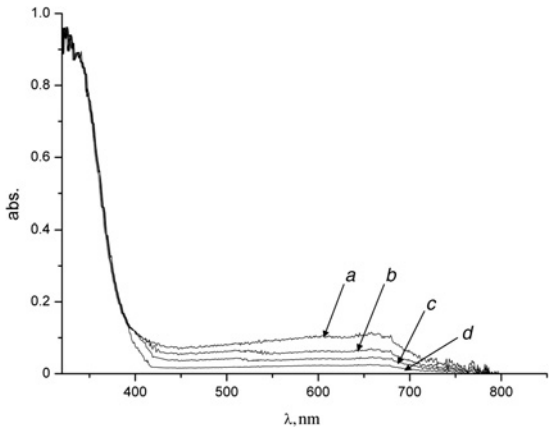

Figure 3 *Diffuse reflectance UV–vis absorption spectra of the TiO_2–NPs samples*
a Doped with 12% MoS_2
b Doped with 7.1% MoS_2
c Doped with 5.6% MoS_2
d Doped with 2.3% MoS_2

Alternatively, the beneficial effects can be quantified in terms of a synergy factor R (1) defined by Matos *et al.* [28]

$$R = \frac{k_{app}(TiO_2 - MoS_2)}{k_{app}(TiO_2)} \quad (1)$$

where k_{app} is taken as the apparent first-order rate constant.

Photodecolourisation activity measurements were carried out in a photocatalytic reactor consisting of a 1-litre quartz vessel (diameter = 12 cm) with two valves (air entrance and purge), a sample collector and two UV lamps (Philips TL8W (Hg), maximum emission at 360 nm). The lamps are cylindrical (30 × 15 cm) and the separation between their centres is 7 cm. Given its environmentally harmful character and widespread use in the textile industry, MB was chosen as our model molecule in order to test the ability of the prepared MoS_2–TiO_2–NPs to decompose organic molecules.

After checking there was no MB degradation under UV radiation without TiO_2 and in the presence of TiO_2 without UV radiation, 300 ml of a 5 ppm MB aqueous solution was introduced into the reactor together with 100 mg of the tested reactant (the different produced MoS_2–TiO_2–NPs samples and the commercial TiO_2 (P25), respectively). Prior to the measurement, the mixture was stirred in darkness at 250 rpm for 30 min to assure reactant surface saturation with the MB (Fig. 4). The solutions were subsequently aerated and illuminated by the UV lamps. 3 ml samples were regularly extracted and filtered. The MB degradation was followed by UV–vis absorption spectroscopy at 662 nm.

The reaction followed apparent first-order kinetics, in agreement with the generally observed Langmuir–Hinshelwood kinetics

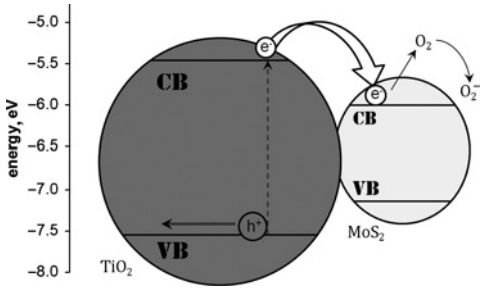

Figure 5 *Schematic representation for the redox potential of the valence (VB) and conduction bands (CB) of the TiO_2–NP and the MoS_2–NP for the prepared hybrid nanomaterials*

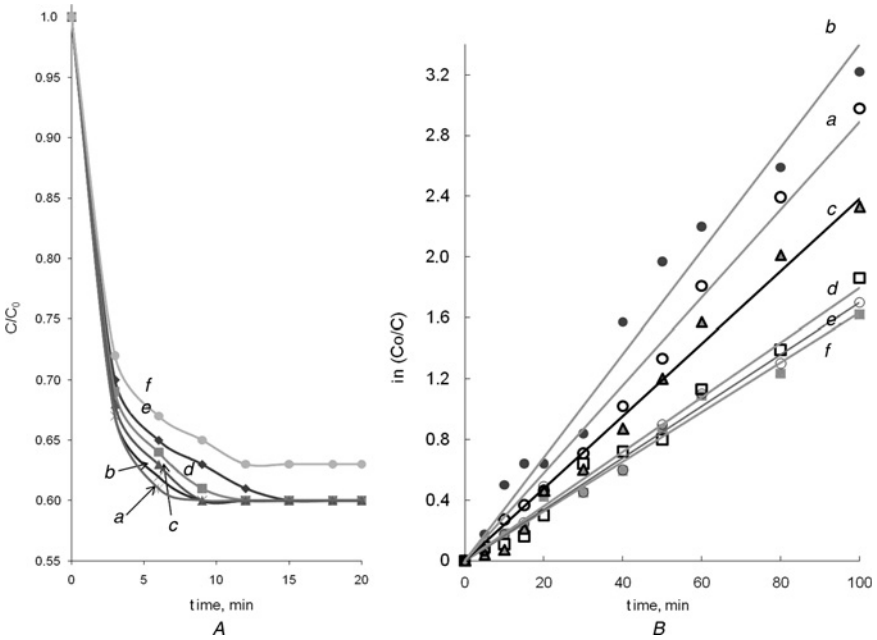

Figure 4 *(A) Rates of photocatalysed degradation of the MB aqueous solutions under a simulated solar irradiation and (B) adsorption in darkness of MB*
a Doped with 12% MoS_2
b Doped with 7.1%
c Doped with 5.6%
d Doped with 2.3%
e Doped with 0%
f P25

doi: 10.1049/mnl.2011.0460

model:

$$r = \frac{dc}{dt} = \frac{kKc}{1 + KC} \quad (2)$$

This equation can be simplified to an apparent first-order equation

$$\ln\left(\frac{c}{c_o}\right) = kKt = k_{app}t \quad (3)$$

with k_{app} being the first-order rate constant. The results of these experiments are plotted in Fig. 5 and the apparent first-order rate constants, k_{app} [min^{-1}], are shown in Table 1. To confirm that the loss of colour observed during the photocatalysis experiments was due to the mineralisation of the MB instead of the photoreduction of the MB to leuco-MB (which is also colourless), the purged gases from the photoreactor were blown through a H_2O adsorber and CO_2 adsorber consecutively. The powders resulting from the CO_2 adsorption (containing the adsorbing material and the adsorbed CO_2) were characterised using the previously mentioned elemental analysis equipment. The increase in carbon content with respect to the raw adsorber allowed us to calculate the mineralisation percentage obtained with each tested photocatalyst material after 100 min operation. These results are listed in Table 1 where the percentage of mineralisation can be compared with the degradation percentages. A mineralisation level of 43% was obtained after 100 min with the 7.1% MoS_2, compared with the 7% reached by the Degussa P-25 reaching under the same experimental conditions

The synergy R factors calculated using expression (1) for the different tested samples are also listed in Table 1. It was observed that the R factors corresponding to the MoS_2–TiO_2–NPs samples are always higher than the R factor of P25 (equal to the unit), reaching the highest value ($R = 2.125$) for the sample containing 7.1% MoS_2.

By comparison with the commercial TiO_2 (P25), the hybrid MoS_2–TiO_2 materials always showed an increase in the reaction rate, doubling its value with the optimum content of MoS_2 (7.1%). Since no red shift was detected in the anatase bandgap, we assumed that the improvement in the photocatalytic activity of the MoS_2–TiO_2–NPs could be explained by the inter-particle electron transfer from irradiated anatase crystal to the MoS_2 conduction band (CB) [29], as has been schematically represented in Fig. 6. In the MoS_2 conduction band (CB), electrons are scavenged by molecular oxygen O_2 (from air gas) to yield the superoxide radical anion ($^{\bullet}O_2^-$) and the hole remaining in the TiO_2–NPs. This newly formed intermediate ($^{\bullet}O_2^-$) can react to produce ($^{\bullet}OH^-$) (hydroxyl radical ion) [5]. These types of radicals are powerful oxidising agents capable of degrading most pollutants [30]. Therefore this charge transfer enhances the photo-oxidation of the adsorbed organic substrate by isolating electrons and holes in two distinct particles.

Increased content of MoS_2 improves photocatalysis of anatase because MoS_2–NPs allow more electrons to remain separate. However, there is an optimum concentration of MoS_2 after which the reaction rate begins to decrease, since anatase-NPs are responsible for the generation of electron-hole pairs. Excess MoS_2 might compete with TiO_2 for the UV light [31].

4. Conclusions: We have developed an easy method to synthesise hybrid MoS_2–TiO_2 nanomaterials at low temperatures with improved catalytic properties with a significant potential for the photodegradation of organic molecules. MoS_2 nanoparticles anchored on the surface of anatase nanoparticles do not have a reductive effect on the bandgap energy of the hybrid material but are able to remove electrons from the surface of anatase. Thus, the isolation of electron-hole pairs on both crystal surfaces seems to be prolonged, what might explain the enhanced photoreaction of the hybrid material with pollutant organic molecules. The highest photocatalytic activity for the degradation of MB was reached for the MoS_2–TiO_2 sample containing 7.1 wt% of MoS_2. By comparison with the commercial TiO_2 (P25), the hybrid MoS_2–TiO_2 materials always showed an increase in the reaction rate, doubling its value with the optimum content of MoS_2 (7.1%).

5. Acknowledgments: This work was funded by the Government of Aragon and 'La Caixa' Ref. GA-LC-041/2008 and by the Spanish Ministry of Science and Innovation Ref. EUI2008-00152.

6 References

[1] Grätzel M.: 'Solar energy conversion by dye-sensitized photovoltaic cells', *Inorg. Chem.*, 2005, **44**, pp. 6841–6851

[2] Bae E., Choi W.: 'Effect of the anchoring group (carboxylate vs phosphonate) in Ru-complex-sensitized TiO_2 on hydrogen production under visible light', *J. Phys. Chem. B*, 2006, **110**, pp. 4792–4799

[3] Österlund L., Stengl V., Mattsson A., Bakardjieva S., Andersson P.O., Oplustil F.: 'Effect of sample preparation and humidity on the photodegradation rate of CEES on pure and Zn-doped anatase TiO_2 nanoparticles prepared by homogeneous hydrolysis', *Appl. Catal. B*, 2009, **88**, pp. 194–203

[4] Arami H., Mazloumi M., Khalifehzadeh R., Sadrnezhaad S.K.: 'Sonochemical preparation of TiO_2 nanoparticles', *Mater. Lett.*, 2007, **67**, pp. 4559–4561

[5] Carp O., Huisman C.L., Reller A.: 'Photoinduced reactivity of titanium dioxide', *Progr. Solid State Chem.*, 2004, **32**, pp. 33–177

[6] Bessekhouad Y., Robert D., Weber J.V.: 'Preparation of TiO_2 nanoparticles by sol–gel route', *Int. J. Photoener.*, 2003, **5**, pp. 153–158

[7] Testino A., Bellobono I.R., Buscaglia V., *ET AL.*: 'Optimizing the photocatalytic properties of hydrothermal TiO_2 by the control of phase composition and particle morphology: a systematic approach', *J. Am. Chem. Soc.*, 2007, **129**, pp. 3564–3575

[8] Rajeshwar K.: 'Photoelectrochemistry and the environment', *J. Appl. Electrochem.*, 1995, **25**, pp. 1067–1082

[9] Subramanian V., Wolf E., Kamat P.V.: 'Semiconductor–metal composite nanostructures. To what extent do metal nanoparticles improve the photocatalytic activity of TiO_2 films?', *J. Phys. Chem. B*, 2001, **105**, pp. 11439–11446

[10] Chen C., Wang Z., Ruan S., Zou B., Zhao M., Wu F.: 'Photocatalytic degradation of C.I. acid orange 52 in the presence of Zn-doped TiO_2 prepared by a stearic acid gel method', *Dyes Pigments*, 2008, **77**, pp. 2204–2209

[11] Liu Y., Chen X., Li J., Burda C.: 'Photocatalytic degradation of azo dyes by nitrogen-doped TiO_2 nanocatalysts', *Chemosphere*, 2005, **61**, pp. 11–18

[12] Zhang Y.J., Yan W., Wu Y.P., Wang Z.H.: 'Synthesis of TiO_2 nanotubes coupled with CdS nanoparticles and production of hydrogen by photocatalytic water decomposition', *Mater. Lett.*, 2008, **62**, pp. 3846–3848

[13] Zhu J., Zheng W., He B., Zhang J., Anpo M.: 'Characterization of Fe–TiO_2 photocatalysts synthesized by hydrothermal method and their photocatalytic reactivity for photodegradation of XRG dye diluted in water', *J. Mol. Catal. A*, 2004, **216**, pp. 35–43

[14] Sökmen M., Allen D.W., Akkas F., Kartal M., Acar F.: 'Photodegradation of some dyes using Ag-loaded titaniumdioxide', *Water Air Soil Pollut.*, 2001, **132**, pp. 153–163

[15] Hamal D.B., Klabunde K.J.: 'Synthesis, characterization, and visible light activity of new nanoparticle photocatalysts

based on silver, carbon, and sulfur-doped TiO_2', *J. Colloid Interf. Sci.*, 2007, **311**, pp. 514–522
[16] Li Z., Shen W., He W., Zu X.: 'Effect of Fe-doped TiO_2 nanoparticle derived from modified hydrothermal process on the photocatalytic degradation performance on methylene blue', *J. Hazard Mater.*, 2008, **155**, pp. 590–594
[17] Wang S., Gong Q., Liang J.: 'Sonophotocatalytic degradation of methyl orange by carbon nanotube/TiO_2 in aqueous solutions', *Ultrason. Sonochem.*, 2009, **16**, pp. 205–208
[18] Bessekhouad Y., Robert D., Weber J.V.: 'Bi_2S_3/TiO_2 and CdS/TiO_2 heterojunctions as an available configuration for photocatalytic degradation of organic pollutant', *J. Photochem. Photobiol. A Chem.*, 2004, **163**, pp. 569–580
[19] Kanda S., Akita T., Fujishima M., Tada H.: 'Facile synthesis and catalytic activity of MoS_2/TiO_2 by a photodeposition-based technique and its oxidized derivative MoO_3/TiO_2 with a unique photochromism', *J. Colloid Interf. Sci.*, 2011, **354**, pp. 607–10
[20] Coehoorn R., Haas C., de Groot R.A.: 'Electronic structure of $MoSe_2$, MoS_2, and WSe_2. II. The nature of the optical band gaps', *Phys. Rev. B*, 1987, **35**, pp. 6203–6206
[21] Hu K.H., Liu Z., Huang F., Hu X.H., Han C.L.: 'Synthesis and photocatalytic properties of nano-MoS_2/kaolin composite', *Chem. Eng. J.*, 2010, **162**, pp. 836–843
[22] Thurston T.R., Wilcoxon J.P.: 'Photooxidation of organic chemicals catalyzed by nanoscale MoS_2', *J. Phys. Chem. B*, 1999, **103**, pp. 11–17
[23] Sobczynski A.: 'Molybdenum-disulfide as a hydrogen evolution catalyst for water photodecomposition on semiconductors', *J. Catal.*, 1991, **131**, pp. 156–166
[24] Linsbigler A.L., Lu G.Q., Yates Jr. J.T.: 'Photocatalysis on TiO_2 surfaces: principles, mechanisms, and selected results', *Chem. Rev.*, 1995, **95**, pp. 735–758
[25] Tacchini I., Terrado E., Ansón A., Martínez M.T.: 'Anatase nanotubes synthesized by a template method and their application as a green photocatalyst', *J. Mater. Sci.*, 2011, **46**, pp. 2097–2104
[26] Wu C.D., Wei D.B., Fan J.C., Wang L.S.: 'Photosonochemical degradation of trichloroacetic acid in aqueous solution', *Chemosphere*, 2001, **44**, pp. 1293–1297
[27] Faria J.L., Wang W., Serp P., Figueiredo J.L.: 'Carbon materials for catalysis' (Wiley, Hoboken, NJ, 2009), pp. 481–506
[28] Matos J., Laine J., Herrmann J.M.: 'Association of activated carbons of different origins with titania in the photocatalytic purification of water', *Carbon*, 1999, **37**, pp. 1870–1872
[29] Fujishima A., Hashimoto A., Watanabe T.: 'TiO_2 photocatalysis: fundamentals and applications' (Koyo printing Co., Japan, 1999)
[30] Bard A.J., Parsons R.: 'Standard potentials in aqueous solution' (Jordan, 1985)
[31] Yu Y., Yu J.C., Kwok Y., Che Y., Zhao J., Ding L.: 'Enhancement of photocatalytic activity of mesoporous TiO_2 by using carbon nanotubes', *Appl. Catal. A Gen.*, 2005, **289**, pp. 186–196

doi: 10.1049/mnl.2011.0460